Nuclear Engineering and Technology 53 (2021) 1947–1954

Contents lists available at ScienceDirect

Nuclear Engineering and Technology

journal homepage: www.elsevier.com/locate/net

Original Article

Similarity analysis of pixelated CdTe semiconductor gamma camera image using a quadrant bar phantom for nuclear medicine: Monte Carlo simulation study

Chan Rok Park [a], Seong-Hyeon Kang [b], Youngjin Lee [b, *]

[a] Department of Radiological Science, Jeonju University, 303, Cheonjam-ro, Wansan-gu, Jeonju, Republic of Korea
[b] Department of Radiological Science, Gachon University, 191, Hambakmoero, Yeonsu-gu, Incheon, Republic of Korea

ARTICLE INFO

Article history:
Received 15 June 2020
Received in revised form
30 November 2020
Accepted 9 December 2020
Available online 13 December 2020

Keywords:
Monte Carlo simulation
Quadrant bar phantom for quality control
Similarity analysis
Pixelated cadmium telluride semiconductor detector
Nuclear medicine imaging system

ABSTRACT

In the nuclear medicine imaging, quality control (QC) process using quadrant bar phantom is fundamental aspect of evaluating the spatial resolution. In addition, QC process of gamma camera is performed by daily or weekly. Recently, Monte Carlo simulation using the Geant4 application for tomographic emission (GATE) is widely applied in the pre-clinical nuclear medicine field for modeling gamma cameras with pixelated cadmium telluride (CdTe) semiconductor detector. In this study, we modeled a pixelated CdTe semiconductor detector and quadrant bar phantom (0.5, 1.0, 1.5, and 2.0 mm bar thicknesses) using the GATE tool. Similarity analysis based on correlation coefficients and peak signal-to-noise ratios was performed to compare image qualities for various source to collimator distances (0, 2, 4, 6, and 8 cm) and collimator lengths (0.2, 0.4, 0.6, 0.8, and 1.0 cm). To this end, we selected reference images based on collimator length and source to collimator distance settings. The results demonstrate that as the collimator length increases and the source to collimator distance decreases, the similarity to reference images improves. Therefore, our simulation results represent valuable information for the modeling of CdTe-based semiconductor gamma imaging systems and QC phantoms in the field of nuclear medicine.

1. Introduction

Monte Carlo simulation tools utilize random variables to perform numerical estimation [1]. In particular, the Geant4 application for tomographic emission (GATE) has been used extensively for modeling nuclear physics and developing reconstruction algorithms for emission tomography [2–4]. The GATE is useful for modeling new camera designs with varying collimator geometry and detector materials. Additionally, this tool is useful for evaluating the performance of new gamma camera designs prior to manufacturing clinical instrumentation.

Recent studies have suggested that advanced techniques, such as new detector applications with cadmium telluride (CdTe) semiconductors instead of conventional NaI(Tl) scintillators, can provide excellent image performance based on simulations and experiments [5–7]. C. Scheiber et al. indicated that CdTe semiconductor detectors are helpful for improving spatial resolution based on their efficient radiation absorption, high sensitivity, and high stability at room temperature [5]. Additionally, Iida et al. reported that scattered photons in pixelated semiconductor detectors are smaller than those in non-pixelated NaI(Tl) scintillation detectors [6]. S. J. Park et al. reported that gamma camera systems with CdTe semiconductors exhibit improved performance compared to conventional NaI(Tl) scintillation detector systems in terms of spatial resolution based on experiments conducted using a micro-Derenzo phantom and mouse brain images [8]. Overall, the GATE has provided excellent accuracy and reliability in the nuclear medicine field for numerous studies.

In general, the quality control processes in nuclear medicine imaging are performed to improve diagnosis accuracy by applying suitable phantoms for the purpose of daily, weekly, or monthly image evaluation [9,10]. One popular phantom is the quadrant bar phantom, which is commonly used to evaluate spatial resolution. A quadrant bar phantom consists of four groups of lead bars with thicknesses of 2.0, 2.5, 3.0, and 3.5 mm, respectively, that cover a total area of 56.5 × 43.2 cm^2. B. Kasal reported that the estimation of spatial resolution from the full width at half maximum (FWHM) using a point spread function (PSF) in a gamma image based on a

* Corresponding author.
E-mail address: yj20@gachon.ac.kr (Y. Lee).

https://doi.org/10.1016/j.net.2020.12.010

bar phantom is a useful and essential process in the nuclear medicine field prior to scanning patients [11]. However, there have been few simulation studies on the evaluation of image quality according to various gamma instrumentation geometries by using quadrant bar phantoms to estimate spatial resolution. Therefore, the goal of this study was to evaluate the similarity degrees and perform visualization evaluations between reference and comparison images according to changes in source to collimator distance (0, 2, 4, 6, and 8 cm) and collimator length (0.2, 0.4, 0.6, 0.8, and 1.0 cm). To this end, we designed a pixelated CdTe semiconductor detector and quadrant bar phantom using the GATE. To perform similarity analysis and set reference images, the FWHM with a PSF for spatial resolution was adopted. Correlation coefficients (CCs) and peak signal-to-noise ratios (PSNRs) are used to evaluate the similarity degree between reference and comparison images.

2. Materials and methods

2.1. Gamma camera detector simulation

In this study, we implemented simulations using the GATE version 8.0 to compare image quality with respect to gamma images. Fig. 1 presents a diagram of the implemented gamma camera system. The pixelated CdTe photoionization detector was modeled by using the GATE. Fig. 2 presents a schematic illustration of the experimental setup used in this study [12]. The detector consists of 51.2 × 51.2 mm of CdTe semiconductor material with a thickness of 3 mm. The matrix size of the images is 128 × 128 with a 0.4 mm pixel size and 10% energy window of 140 keV (^{99m}Tc). The collimator geometry affects imaging performance. Fig. 3 presents the main parameters determining collimator performance. The collimator hole length and diameter are crucial parameters affecting the collimator resolution (R_c) and efficiency (ε_c) [13,14].

$$R_C = d\frac{\left(l_{eff}+z\right)}{l_{eff}} \quad (1)$$

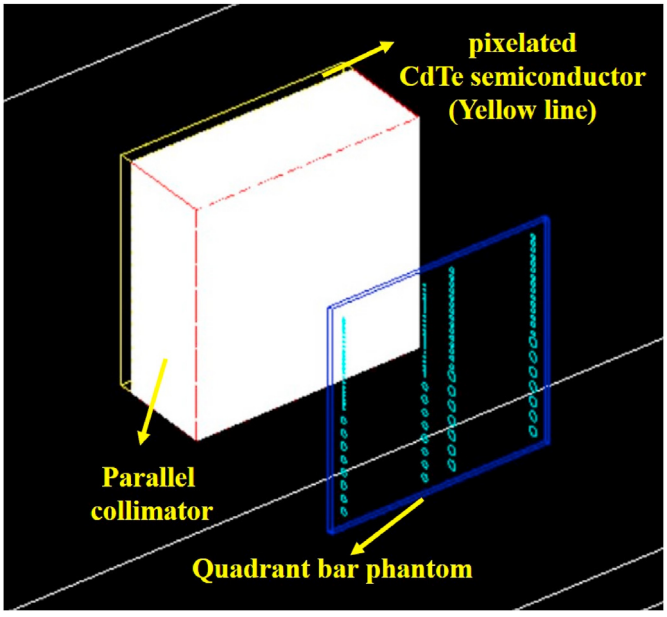

Fig. 1. Diagram of a gamma camera modeling system with a pixelated CdTe semiconductor, pixelated collimator, and quadrant bar phantom based on the GATE.

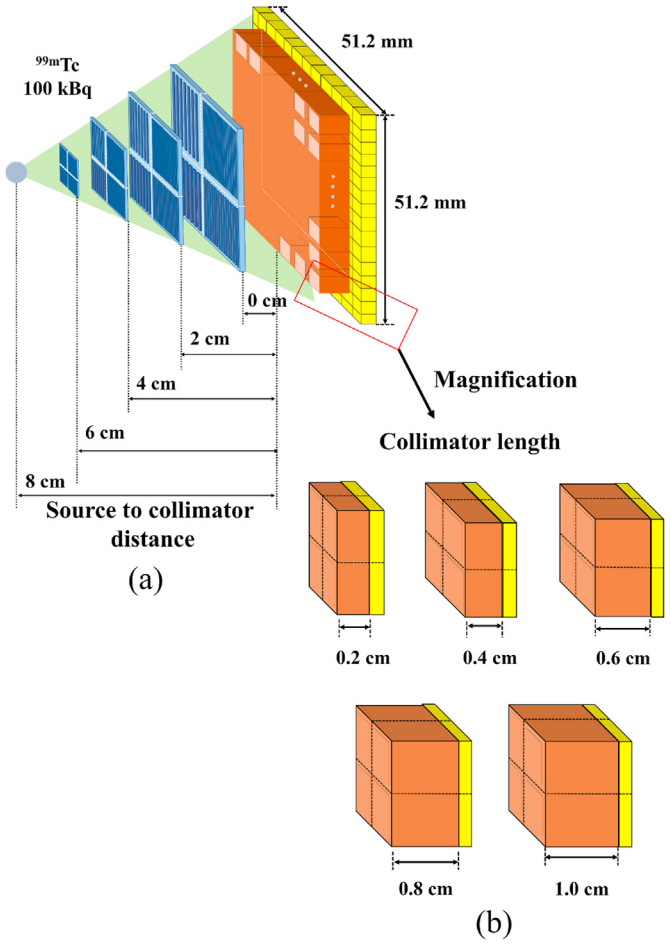

Fig. 2. Schematic illustration of a pixelated CdTe semiconductor detector system, including (a) various source-to-collimator distances (0, 2, 4, 6, and 8 cm) and (b) collimator lengths (0.2, 0.4, 0.6, 0.8, and 1.0 cm), based on a quadrant bar phantom modeled using the GATE.

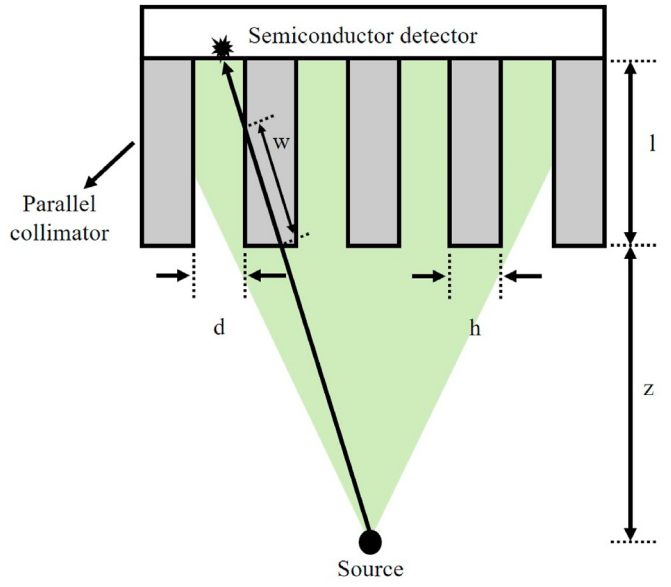

Fig. 3. Schematic diagram of a gamma ray following the shortest path (w) through a parallel collimator with various parameters for determining image quality.

$$\varepsilon_c = K^2\left(\frac{d}{l_{eff}}\right)^2 \frac{d^2}{(d+h)^2} \quad (2)$$

where d and z are the hole diameter and source to collimator distance, respectively; l_{eff} is the effective length of the collimator holes, which is defined as $l_{eff} = l - 2 \times \mu^{-1}$, where μ is the linear attenuation coefficient of the collimator material; l is the collimator length; and K and h are constants representing the hole shape and septal thickness, respectively.

Additionally, the primary consideration for collimator design is ensuring the penetration of gamma rays according to the collimator septal thickness. The septal thickness (t) in a collimator is calculated as follows:

$$t = \frac{2dw}{(l-w)} \quad (3)$$

where w is the minimum path length. The septal thickness in a collimator generally is designed such that approximately 5% of gamma rays penetrate along the shortest septal path.

$$e^{-\mu w} \leq 0.05 \quad (4)$$

In this study, a tungsten collimator material was used based on its suitable cost and availability (Z = 74, ρ = 19.3 g/cm^3). Consequently, the septal thickness is related to the linear attenuation coefficient as follows [15]:

$$t \geq \frac{\frac{6d}{\mu}}{l - \left(\frac{3}{\mu}\right)} \quad (5)$$

To model a parallel low-energy high-resolution collimator. which has the same hole and pixel size, the tungsten collimator was arranged by repeating the square array (0.35 × 0.35 mm) of the hole size and the 0.05 mm septal thickness. The collimator length was 2 cm. To evaluate performance in terms of spatial resolution using the GATE, we modeled a quadrant bar phantom. A diagram of the quadrant bar phantom specifications is presented in Fig. 4. The phantom contains four different thicknesses (0.5, 1.0, 1.5, and 2.0 mm) of rectangular bar shapes with a width and length of 18.75 × 10 mm, respectively. The total size of the phantom containing all bars is 50 × 50 mm. The phantom images were acquired under various simulation conditions using the ^{99m}Tc with a radioactivity of 1 MBq over 500 s of acquisition time. We evaluated image quality using the quadrant bar phantom from two perspectives. First, images were captured with various distances from the source to collimator (0, 2, 4, 6, and 8 cm). Second, the collimator length was considered (0.2, 0.4, 0.6, 0.8, and 1.0 cm). To evaluate image quality based on similarity methods, which is a form of quantitative analysis (e.g., CC and PSNR), reference images were selected by measuring the FWHM using the PSF of the point source, which outputted 1 MBq of radioactivity and had a diameter of 1 mm in air with ^{99m}Tc over 900 s of acquisition time. The FWHM was calculated as follows:

$$FWHM = 2\sqrt{2\,log2} \times \sigma \quad (6)$$

where σ is the standard deviation of the Gaussian fitting in the acquired image.

2.2. Quantitative analysis

The similarity methods representing the correlation between reference and comparison images (i.e., CC and PSNR) were calculated as follows:

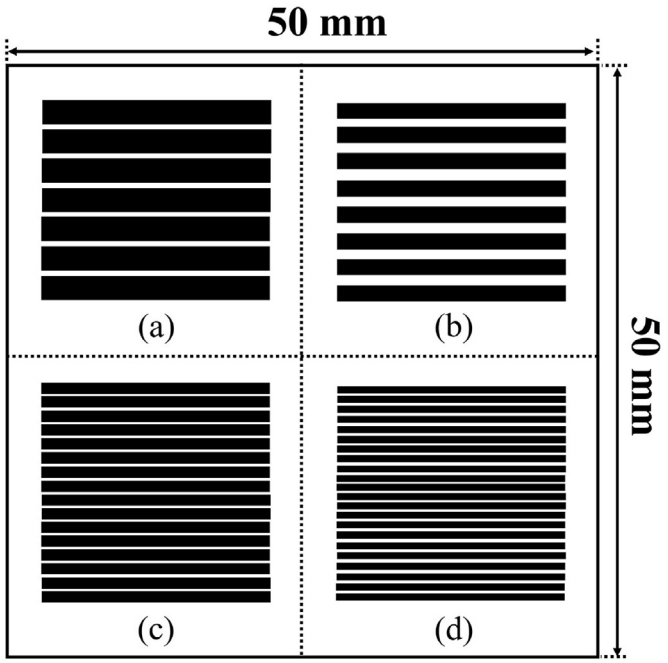

Fig. 4. Quadrant bar phantom diagram. This phantom contains 4 bar thicknesses (number of bars = (a) 2 mm: 7 bars, (b) 1.5 mm: 8 bars, (c) 1.0 mm: 16 bars, and (d) 0.5 mm: 22 bars) that are filled with ^{99m}Tc over 500 s. The sizes of all bars are the same at 18.75 × 10 mm^2 in width and length, respectively.

$$CC = \frac{\sum_{i=1}^{N}(f(i,j) - \overline{f(i,j)}) \times (g(i,j) - \overline{g(i,j)})}{\sqrt{\sum_{i=1}^{N}(f(i,j) - \overline{f(i,j)})^2}\sqrt{\sum_{i=1}^{N}(g(i,j) - \overline{g(i,j)})^2}} \quad (7)$$

$$MSE = \frac{1}{N}\sum_{j=1}^{N}[f(i,j) - g(i,j)]^2 \quad (8)$$

$$PSNR = 10log\frac{{f_{peak}}^2}{MSE} \quad (9)$$

where $f(i,j)$ and $g(i,j)$ are the pixel values of the reference and comparison images, respectively, N represents the size of each pixel, f_{peak} is the maximum pixel value in the image, and $\overline{f(i,j)}$ and $\overline{g(i,j)}$ are the mean values of the reference and comparison images, respectively.

3. Results

Fig. 5 presents the results for the FWHM for calculating spatial resolution. Regarding the FWHM results obtained using the aforementioned point source for the reference images, Fig. 6 reveals that the FWHM results for source to collimator distances of 0, 2, 4, 6, and 8 cm are 1.10, 1.38, 1.65, 1.92, and 2.18 mm, respectively. Additionally, the FWHM values were 15.52, 2.63, 1.73, 1.42, and 1.24 mm for collimator lengths of 0.2, 0.4, 0.6, 0.8, and 1.0 cm, respectively. Consequently, the reference images were suitable for the 0 cm source to collimator distance and 1.0 cm collimator length based on the FWHM results. The FWHM value at a source to collimator distance of 0 cm is 1.98, 1.57, 1.32, and 1.13 times greater than those at source to collimator distances of 2, 4, 6, and 8 cm, respectively.

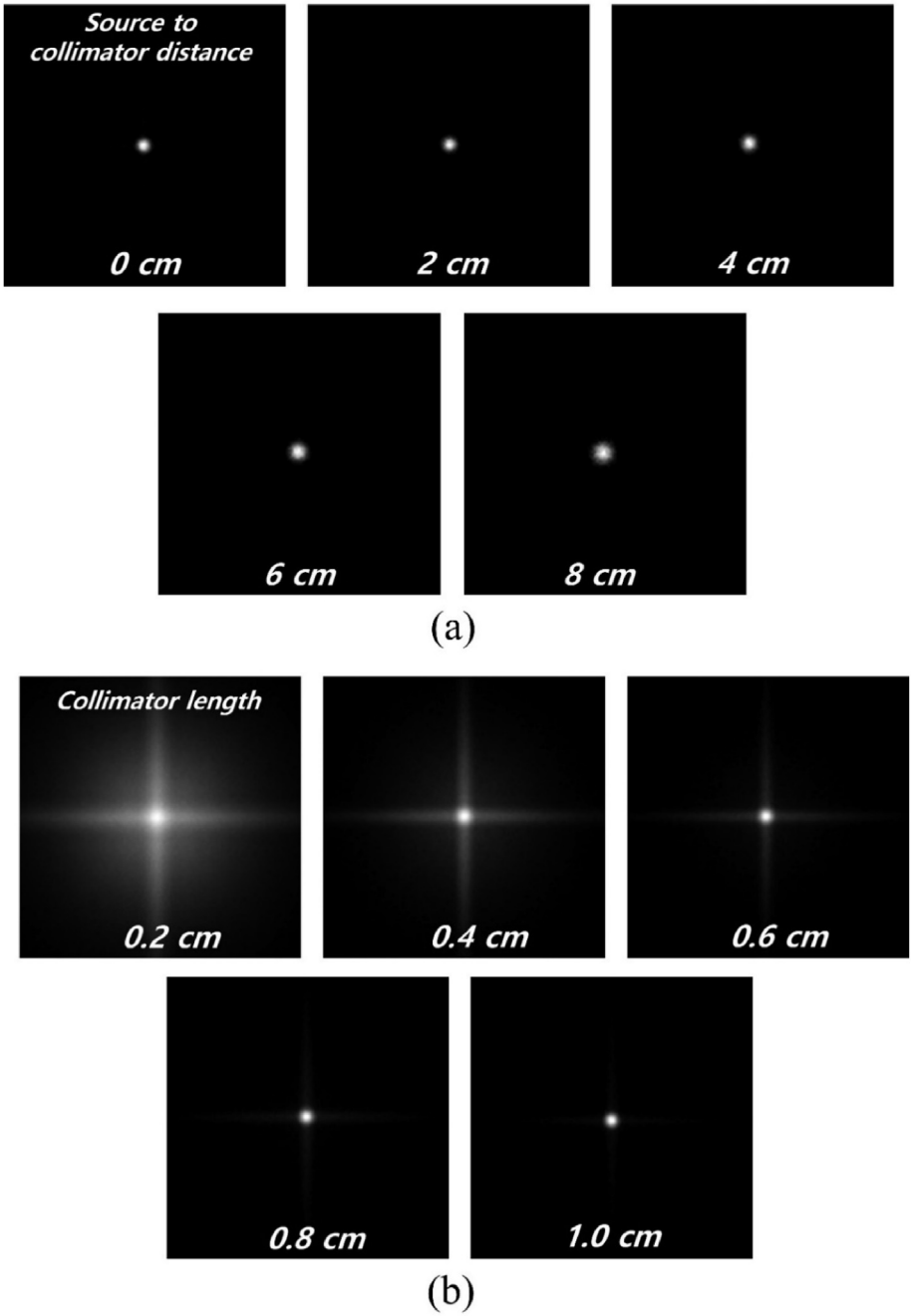

Fig. 5. Images acquired with a point source of ^{99m}Tc with 1 MBq of radioactivity over 900 s using a pixelated CdTe detector system with varying (a) source-to-collimator distances and (b) collimator lengths. These images are used to analyze the similarity between reference and comparison images.

Additionally, the FWHM value at a collimator length of 1.0 cm is 12.51, 2.12, 1.39, and 1.14 times greater than those a collimator lengths of 0.2, 0.4, 0.6, and 0.8 cm, respectively.

Figs. 7 and 8 presents quadrant bar phantom images for various source to collimator distances and collimator lengths. One can see that the images for varying source to collimator distances can be distinguished between the 1.5 and 2.0 mm bars, but not between the 0.5 and 1.0 bars. Additionally, when comparing the images for varying source to collimator distances for the 1.5 and 2.0 mm bars, it is possible to distinguish the bars for source to collimator distances of 0 and 2 cm, whereas in the images for the other conditions (4, 6, and 8 cm), it is difficult to confirm the separation of the bars through visual evaluation. In particular, in the image for the source to collimator distance of 8 cm, it is not possible to not separate all bars. When comparing the images according to collimator length, it is not possible to distinguish the 0.5 and 1.0 mm bars. The images of the 1.5 and 2.0 mm bars are relatively more distinguishable.

Figs. 9 and 10 present similarity results in terms of CCs and PSNRs evaluated using reference images with a source to collimator distance of 0 cm and collimator length of 1.0 cm. The CC results for source to collimator distances of 2, 4, 6, and 8 cm are 0.99, 0.53, 0.52, and 0.05, respectively. Those for collimator lengths of 0.2, 0.4, 0.6, and 0.8 cm are 0.88, 0.90, 0.92, and 0.94, respectively. The PSNR results for source to collimator distances of 2, 4, 6, and 8 cm are 6.84, 4.34, 4.37, and 4.40, respectively. Those for collimator lengths of 0.2, 0.4, 0.6, and 0.8 cm are 68.82, 85.45, 99.82, and 114.01,

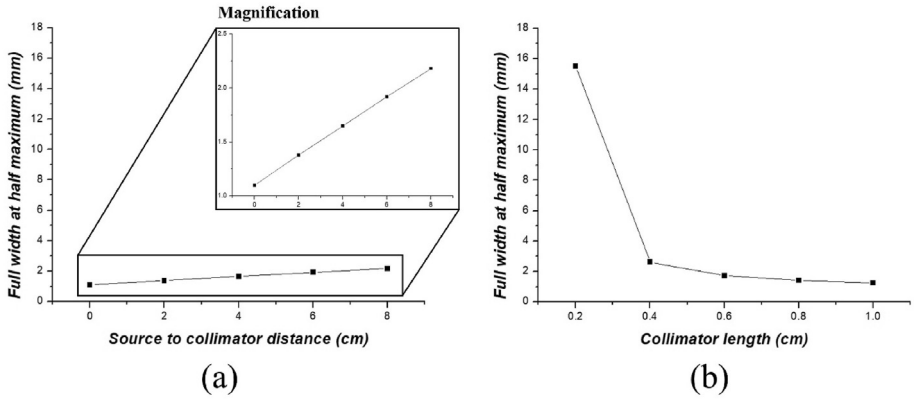

Fig. 6. Results for FWHM values of the PSF for the spatial resolution of pixelated CdTe detector systems according to (a) source-to-collimator distance and (b) collimator length.

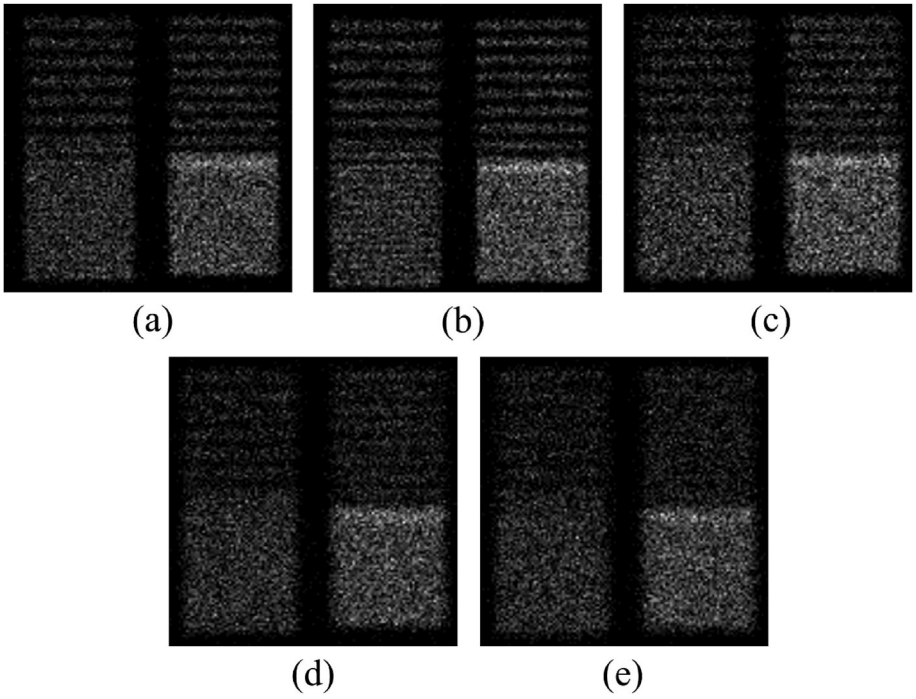

Fig. 7. Result images for quadrant bar phantoms simulated with respect to source-to-collimator distance with a collimator length of 2 cm: (a) 0, (b) 2, (c) 4, (d) 6, and (e) 8 cm. The phantom images represent different bar thicknesses of 2 (top left), 1.5 (top right), 1.0 (bottom left), and 0.5 mm (bottom right).

respectively. These results indicate that images with a source to collimator distance of 2 cm and collimator length of 0.8 cm yield the best similarity results when compared to the reference images.

4. Discussion

The GATE is a powerful software tool developed by the international OpenGATE collaboration [16]. Recently, there has been increased demand for semiconductor detectors in the nuclear medicine field. The use of pixelated CdTe semiconductor detectors in gamma cameras has led to significant improvements compared to NaI(Tl) conventional scintillation detectors in terms of spatial resolution based on the high stopping power and atomic number of CdTe. Lee et al. proved that pixelated CdTe semiconductor detector systems provide improved spatial resolution compared to hexagonal collimator systems using the GATE [17]. Unlike previous studies, we modeled and acquired gamma images of quadrant bar phantoms, which are used for spatial resolution evaluation, using pixelated CdTe semiconductor detectors based on the GATE and evaluated image performance based on similarity measures, such as CCs and PSNRs, between reference and comparison images.

One limitation of this study is that there are few gamma camera systems with CdTe semiconductor materials in the clinical field because NaI(Tl) scintillator instrumentation is widely used to acquire images. Simulation studies have drawbacks in terms of the clinical application of gamma camera systems based on the high production costs and complex manufacturing processes of such systems. However, we assume that our experimental data will aid in the acquisition of improved image quality in the future.

We confirmed that the collimator septal thickness according to the collimator length is an important parameter for obtaining accurate gamma images because star artifacts are caused by the penetration of gamma rays. Table 1 summarizes the minimum septal thickness results for the target collimator material for

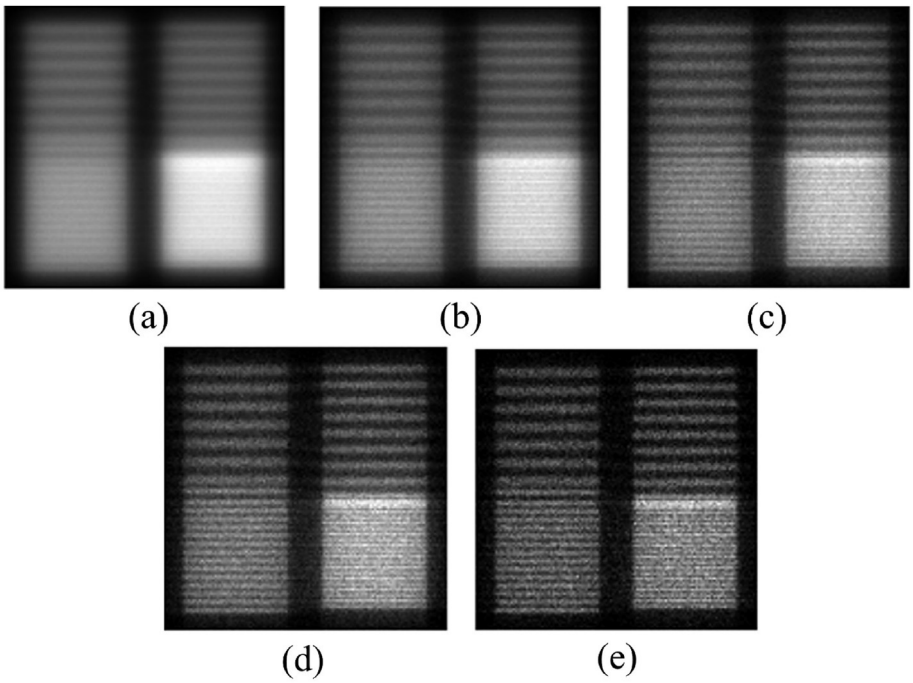

Fig. 8. Result images for quadrant bar phantoms simulated with respect to collimator length: (a) 0.2, (b) 0.4, (c) 0.6, (d) 0.8, and (e) 1.0 cm. The phantom images represent different bar thicknesses of 2 (top left), 1.5 (top right), 1.0 (bottom left), and 0.5 mm (bottom right).

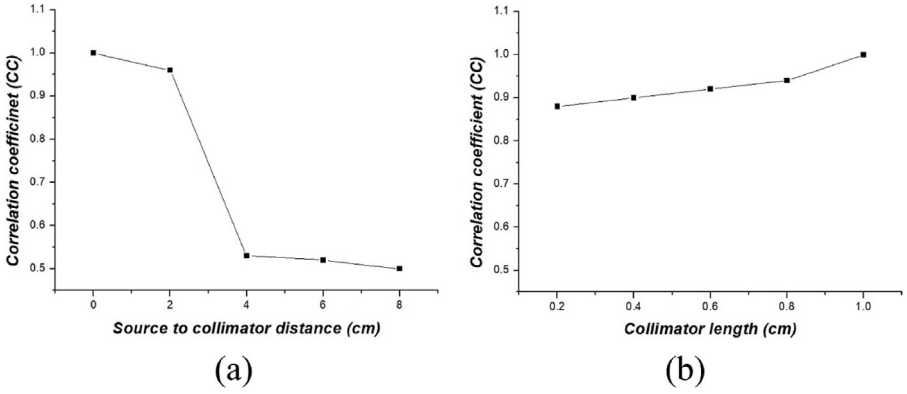

Fig. 9. Comparison of CC results according to (a) source-to-collimator distance and (b) collimator length.

collimator lengths of 0.2, 0.4, 0.6, 0.8, 1.0, and 2.0 cm with a hole size of 0.35 mm. Star artifacts occur in images with collimator lengths of 0.2, 0.4, 0.6, and 0.8 cm based on the calculation results for minimum septal thickness, which is a parameter that determines the penetration of gamma rays in a collimator. The image for the collimator length of 1.0 cm contains no star artifacts. Kobayashi et al. demonstrated that accurate diagnosis may be limited by the occurrence of star artifacts, which make it difficult to identify the locations of metastases [18]. Therefore, we believe that maintaining a proper balance between collimator length and septal thickness when designing collimator geometry is essential for improving image quality.

Based on the CC and PSNR results, as the source to collimator distance increases, spatial resolution decreases. Additionally, as the collimator length increases, spatial resolution also increases. When comparing the CC and PSNR results for the source to collimator distance of 2 cm to those for source to collimator distances of 4, 6, and 8 cm, one can see differences 1.71, 1.74, and 1.78 times, respectively, for CC in Fig. 8(a), and 1.57, 1.57, and 1.55 times, respectively, for PSNR in Fig. 9(a). When comparing the CC and PSNR results for the collimator length of 0.8 cm to those for collimator lengths of 0.2, 0.4, and 0.6 cm, one can see differences of 1.06, 1.05, and 1.02 times, respectively, for CC in Fig. 8(b), and 1.65, 1.33, and 1.14 times, respectively, for PSNR in Fig. 9(b). In summary, we confirmed that image quality is improved when the source to collimator distance decreases and the collimator length increases.

Recently, many researchers have recommended the application of pixelated semiconductor detectors, such as cadmium zinc telluride or CdTe, in gamma camera systems [19,20] because such systems have higher intrinsic spatial resolutions than conventional NaI(Tl) scintillation systems. Lee et al. reported that CdTe-based semiconductor detector systems enhance spatial resolution compared to conventional detector systems by modeling hot-rod phantoms [19]. Additionally, scattering, attenuation, and statistical fluctuation are generated when capturing gamma rays in conventional detector systems. Moreover, Y. Morimoto reported that

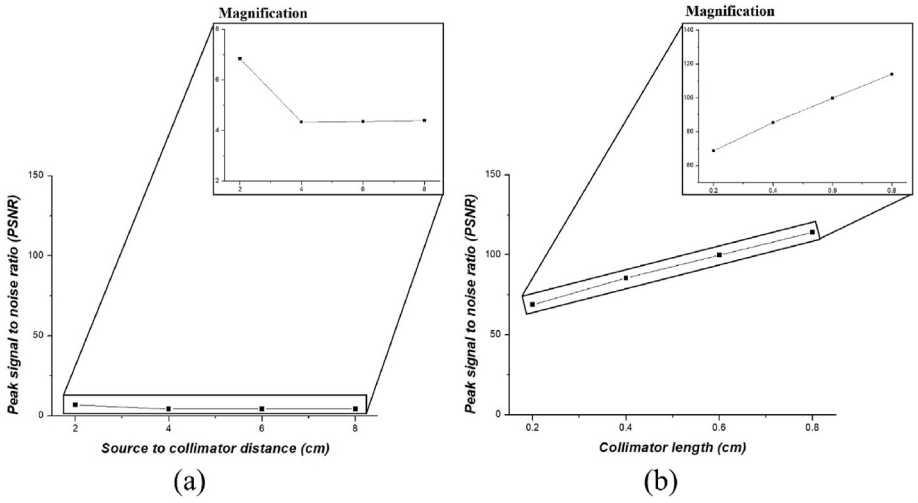

Fig. 10. Comparison of PSNR results according to (a) source-to-collimator distance and (b) collimator length.

Table 1
Calculated minimum septal thicknesses for various collimator lengths with a tungsten (Z = 74, ρ = 19.3 g/cm^3) material at 140 keV.

Linear attenuation coefficient (cm^{-1})	Hole diameter (mm)	Collimator length (cm)	Septal thickness (cm)
30.49	0.354	0.2	0.068
		0.4	0.023
		0.6	0.013
		0.8	0.009
		1.0	0.007
		2.0	0.003

CdTe-based semiconductor material is also effective in the positron emission tomography scanner compared with conventional detector material such as bismuth germanium oxide [21]. In this study, we evaluated image performance according to source to collimator distance and collimator length based for CdTe-based semiconductor detector systems. The usefulness of such systems was verified using quadrant bar phantoms, which are widely used for the evaluation of spatial resolution in gamma image, based on the GATE.

5. Conclusion

In this study, we compared spatial resolutions based on FWHM values for various source to collimator distances and collimator lengths using the GATE by modeling quadrant bar phantoms (0.5, 1, 1.5, and 2 mm bar thicknesses). Similarity analysis based on CCs and PSNRs was performed by comparing reference and comparison images. According to the results, as collimator length increases and source to collimator distance decreases, bars become more clearly separated. Future studies will focus on numerical data, such as modulation transfer functions, for quadrant bar phantoms to express spatial resolution more accurately based on FWHM values. In summary, this study demonstrated the evaluation of spatial resolution using quadrant bar phantoms by modeling CdTe semiconductor detectors based on the GATE.

Declaration of competing interest

The authors declare that they have no known competing financial interests or personal relationships that could have appeared to influence the work reported in this paper.

Acknowledgment

This research was supported by the National Research Foundation of Korea funded by the Ministry of Science and ICT (No. NRF-2019R1F1A1062811).

References

[1] G. Santin, D. Strul, D. Lazaro, L. Simon, M. Krieguer, M.V. Martins, V. Breton, C. Morel, GATE: a geant4-based simulation platform for PET and SPECT integrating movement and time management, IEEE Trans. Nucl. Sci. 50 (2003) 1516–1521.
[2] S. Staelens, D. Strul, G. Santin, S. Bandenberghe, M. Koole, Y. D'Asseler, I. Lemahieu, R. Van de Walle, Monte Carlo simulations of a scintillation camera using GATE: validation and application modeling, Phys. Med. Biol. 48 (2003) 3021–3042.
[3] R. Barquero, H.P. Garcia, m.G. incio, P. Minguez, A. Cardenas, D. Martinez, M. Lassmann, 131I activity quantification of gamma camera planar images, Phys. Med. Biol. 62 (2017) 909–926.
[4] S. Staelens, K. Vunckx, J.D. Beenhouwer, F. Beekman, Y. D'Asseler, J. Nuyts, I. lemahieu, GATE simulations for optimization of pinhole imaging, Nucl. Instrum. Methods A 569 (2006) 359–363.
[5] C. Scheiber, C.C. Giakos, Medical applications of CdTe and CdZnTe detectors, Nucl. Instrum. Methods A 458 (2001) 12–25.
[6] H. Lida, K. Ogawa, Comparison of a pixelated semiconductor detector and a non-pixelated scintillation detector in pinhole SPECT system for small animal study, Ann. Nucl. Med. 25 (2011) 143–150.
[7] K. Ogawa, N. Ohumura, H. Iida, K. Nakamura, T. Nakahara, A. Kubo, Development of an ultra-high resolution SPECT system with a CdTe semiconductor detector, Ann. Nucl. Med. 23 (2009) 763–770.
[8] S.J. Park, A.R. Yu, Y.J. Lee, Y.S. Kim, H.J. Kim, Feasibility of a CdTe-based SPECT for high-resolution low-dose small animal imaging: a Monte Carlo simulation study, J. Inst. Met. 9 (2014) 7001–7018.
[9] M.R. Hasan, H.R. khan, R. Rahman, S. Parvez, R. Islam, A.K. Paul, Quality control of gamma camera with SPECT system, Int. J. Med. Phys. Clin. Eng. Radiat. Oncol. 6 (2017) 225–232.
[10] P.H. Murphy, Acceptance testing and quality control of gamma cameras, including SPECT, J. Nucl. Med. 28 (1987) 1221–1227.
[11] B. Kasal, P.F. Sharp, Gamma camera spatial resolution as measured by the bar phantom, Phys. Med. Biol. 30 (1985) 263–266.

[12] A.F. Resch, A. Elia, H. Fuchs, A. Carlino, H. palmans, M. Stock, D. Georg, Evaluation of electromagnetic and nuclear scattering models in, GATE/Geant4 for proton therapy 46 (2019) 2444–2456.
[13] H. Wieczorek, A. Goedicke, Analytical model for SPECT detector concepts, IEEE Trans. Nucl. Sci. 53 (2006) 1102–1112.
[14] L.S. Graham, Automatic tuning of scintillation cameras: a review, J. Nucl. Med. Technol. 14 (1986) 105–110.
[15] R. Accorsi, S.D. Metzler, Analytic determination of the resolution-equivalent effective diameter of a pinhole collimator, IEEE Trans. Med. Imag. 23 (2004) 750–763.
[16] S. Staelens, D. Strul, G. Santinm, M. Koole, S. Vandenberghe, Y. D'Asseler, I. Lemahieu, R. Van de Walle, Monte Carlo simulations of a scintillation camera using GATE: validation and application modelling, Phys. Med. Biol. 48 (2003) 3021–3042.
[17] Y.J. Lee, H.J. Ryu, H.M. Cho, S.W. Lee, Y.N. Choi, H.J. Kim, Optimization of an ultra-high-resolution parallel-hole collimator for CdTe semiconductor SPECT system, J. Inst. Met. 8 (2013) C01044.
[18] M. Kobayashi, H. Wakabayashi, D. Kayano, T. Konishi, H. Kojima, H. Yoneyama, K. Okuda, H. Tsushima, M. Onoguchi, K. Kawai, S. Kinuya, Application of a medium-energy collimator for I-131 imaging after ablation treatment of differentiated thyroid cancer, Ann. Nucl. Med. 28 (2014) 551–558.
[19] Y.J. Lee, H.J. Ryu, S.W. Lee, S.J. Park, H.J. Kim, Comparison of ultra-high-resolution parallel-hole collimator materials based on the CdTe pixelated semiconductor SPECT system, Nucl. Instrum. Methods A. 713 (2013) 33–39.
[20] T.E. Peterson, L.R. Furenlid, SPECT detectors: the anger camera and beyond, Phys. Med. Biol. 56 (2011). R1445-R182.
[21] Y. Morimoto, Y. Ueno, W. Takeuchi, S. Kojima, K. Matsuzaki, T. Ishitsu, K. Umegaki, Y. Kiyanagi, N. Kubo, C. Katoh, T. Shiga, H. Shirato, N. Tamaki, Development of a 3D brain PET scanner using CdTe semiconductor detectors and its first clinical application, IEEE Trans. Nucl. Sci. 58 (2011) 2181–2189.